ACS NANO
Cite This: ACS Nano 2019, 13, 13317−13324
www.acsnano.org

ARTICLE

Strong Thermopower Enhancement and Tunable Power Factor *via* Semimetal to Semiconductor Transition in a Transition-Metal Dichalcogenide

Hongjae Moon,[†] Joonho Bang,[‡] Seokkyoon Hong,[†] Gwansik Kim,[†] Jong Wook Roh,[§] Jeongmin Kim,*[,†] and Wooyoung Lee*[,†]

[†]Department of Materials Science and Engineering, Yonsei University, 50 Yonsei-ro, Seodaemoon-gu, Seoul 03722, Republic of Korea

[‡]Department of Energy Science, Sungkyunkwan University, Suwon 16419, Republic of Korea

[§]School of Nano and Materials Science and Engineering, Kyungpook National University, Gyeongsangbuk-do 37224, Republic of Korea

Supporting Information

ABSTRACT: **Electronic band engineering is a promising approach to enhance the thermopower of thermoelectric materials. In transition-metal dichalcogenides (TMDCs), this has so far only been achieved using their inherent semiconducting nature. Here, we report the thickness-modulated band engineering of nanosheets based on semimetallic platinum diselenide ($PtSe_2$) resulting in a thermopower enhancement of more than 50 times than that of the bulk. We obtained this by introducing a semimetal to semiconductor (SMSC) transition resulting in the formation of a bandgap. This approach based on semimetallic TMDCs provides potential advantages such as a large variation of transport properties, a decrease of the ambipolar transport effect, and a high carrier density dependence of the transport properties. Our observations suggest that the SMSC transition in TMDCs is a promising and straightforward strategy for the development of two-dimensional nanostructured thermoelectric materials.**

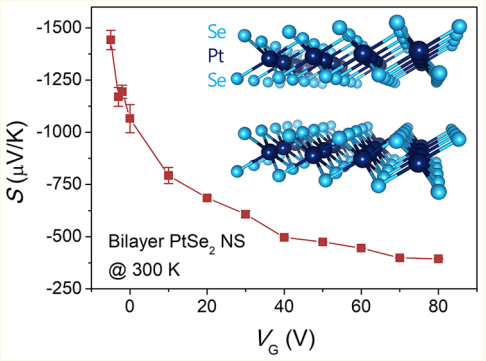

KEYWORDS: *transition-metal dichalcogenides, platinum diselenide, electronic band engineering, semimetal to semiconductor transition, thermopower*

To improve the energy conversion efficiency of thermoelectric materials, significant effort has been placed on developing various nanostructures.[1−3] Crucial properties of a thermoelectric material are the thermopower, also referred to as Seebeck coefficient S, and the electrical conductivity σ.[4] To achieve a significant enhancement of the thermoelectric power factor ($S^2\sigma$), it has first been proposed to use one- and two-dimensional bismuth structures and take advantage of their quantum confinement effect on electrons.[5,6] However, it has been gradually recognized that to boost thermoelectric performance, it is easier and more robust to suppress the thermal conductivity of a material using phonon scattering at interfaces and boundaries in nanostructures.[7−10] Another approach to enhance the power factor is to alter the electronic band structures of a material by nanostructuring, which is called band engineering.[11−17] In particular, one-dimensional semiconducting and semimetallic nanowires have been intensively investigated[12,13] because the thermopower is extremely sensitive to band structures and the asymmetries of electrons and holes in materials.[14] However, only few studies have demonstrated a thermopower enhancement using nanowires beyond that of the bulk material.[15−17]

Recently, semiconducting two-dimensional transition-metal dichalcogenide (TMDC) nanosheets have attracted great interest to obtain enhanced power factors owing to the presence of intrinsic bandgaps and the potential to modulate the band structures by changing their thickness.[18−24] The power factor enhancement was successfully demonstrated in semiconducting bilayer nanosheets of WSe_2, MoS_2, and black phosphorus using field effect gating, achieving values comparable to that of commercial bulk Bi_2Te_3.[18−20] However,

Received: August 16, 2019
Accepted: October 15, 2019
Published: October 15, 2019

DOI: 10.1021/acsnano.9b06523
ACS Nano 2019, 13, 13317−13324

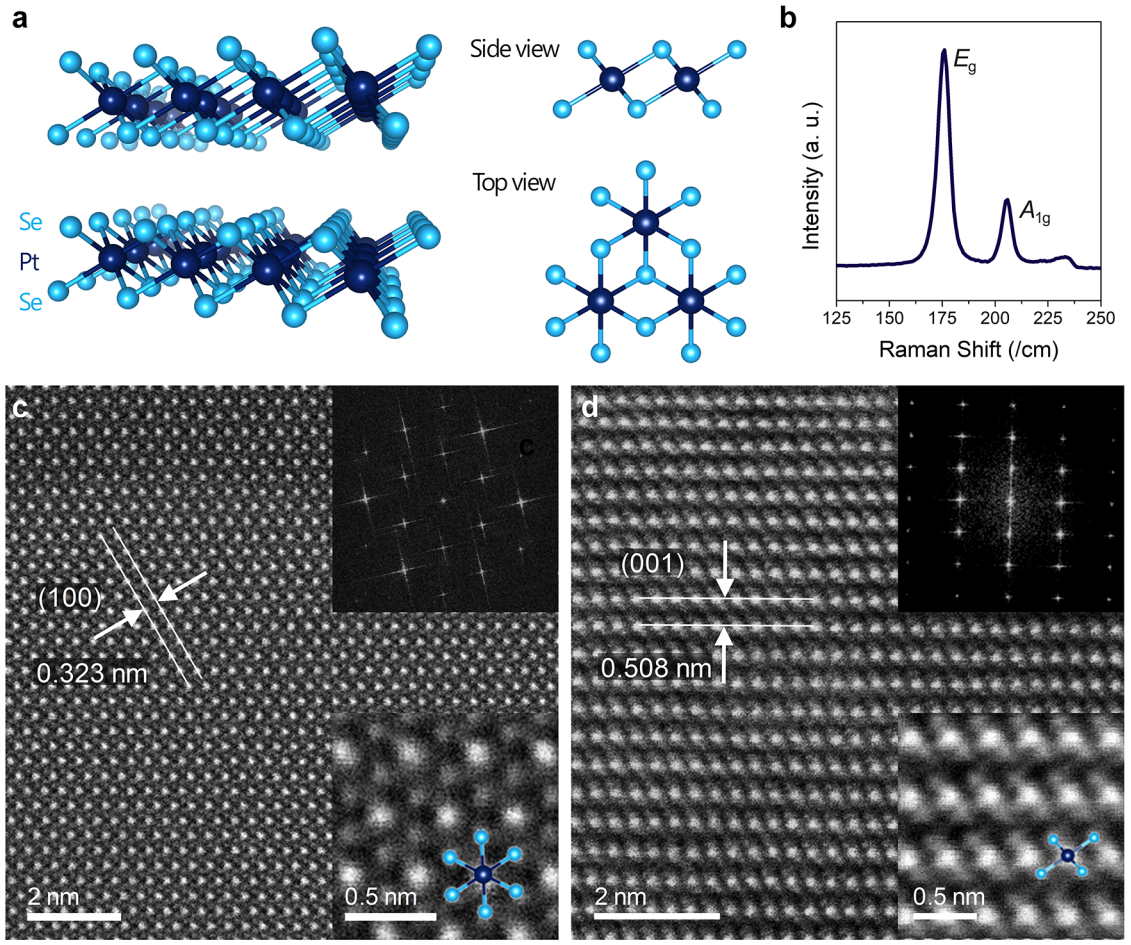

Figure 1. Characterization of the $PtSe_2$ nanosheets. (a) Schematic crystal structure of a bilayer $PtSe_2$ nanosheet (left), and side and top views of the 1T phase $PtSe_2$ crystal structure (right). The dark blue and light blue spheres represent Pt and Se atoms, respectively. (b) Raman spectrum of a $PtSe_2$ nanosheet. (c, d) HR-STEM images of a mechanically exfoliated $PtSe_2$ nanosheet (c) and a cross-sectional specimen (d). The insets are the Fourier transforms of the respective HR-STEM images (top) and the corresponding high-magnification HR-STEM images (bottom).

the thermopower of the nanosheets has not been shown to exceed that of bulk crystals[25,26] even when utilizing the gate effect. Similarly, in theoretical studies based on MoS_2, $MoSe_2$, WS_2, WSe_2, SnS_2, and TiS_2 nanosheets, the power factor was found to increase with decreasing thickness, but the dramatic thermopower enhancement predicted based on their electronic band structure could not be obtained.[21−24] In fact, the power factor enhancement has so far only been observed using field effect gating in 2D semiconducting TMDCs that have an inherently high thermopower.[18−20]

Here, we report on the significant thermopower enhancement in a semimetallic TMDC by introducing a semimetal to semiconductor (SMSC) transition.[6,16] We systematically investigated two-dimensional nanosheets exfoliated from semimetallic platinum diselenide ($PtSe_2$) crystals and obtained thermopowers higher than 1 mV/K. The semiconducting $PtSe_2$ nanosheets obtained by the SMSC transition provide potential advantages in terms of band engineering efficiency for thermoelectric applications. First, the variation of transport properties is exceptionally large compared to that of the bandgap modulation because of the sudden splitting between the overlapping conduction and valence bands. Second, the ambipolar charge carrier transport problem, in which the contributions of electrons and holes to the thermopower offset each other, is diminished by the bandgap formation, and thus, the thermopower enhancement can be further promoted. Third, the transport properties become further sensitive to the intrinsic properties such as carrier density, and thus the thermoelectric properties can be effectively optimized by the field effect gating and extrinsic doping. Our findings represent an approach of thickness-modulated band engineering for thermoelectric applications, which we anticipate to be universally adaptable for semimetallic TMDCs.

RESULTS AND DISCUSSION

Single-Crystalline 1T Phase PtSe2 Nanosheets. $PtSe_2$ nanosheets were obtained using a mechanical exfoliation method on 300 nm SiO_2/Si substrates. Each $PtSe_2$ layer consists of three atomic sublayers, in which platinum (Pt) atoms are sandwiched between selenium (Se) atoms (Figure 1a).[27,28] We performed Raman spectroscopy to confirm the phase of the $PtSe_2$ nanosheets. We observed two pronounced peaks centered around 175 and 206 cm^{-1} (Figure 1b), which correspond to the E_g and A_{1g} Raman active modes originating from the vibration of Se atoms. This is consistent with a previous study on the single-crystalline 1T phase $PtSe_2$.[29] We also observed the infrared active modes A_{2u} and E_u due to vibrations of Pt and Se atoms at around 230 cm^{-1}. In order to

DOI: 10.1021/acsnano.9b06523
ACS Nano 2019, 13, 13317−13324

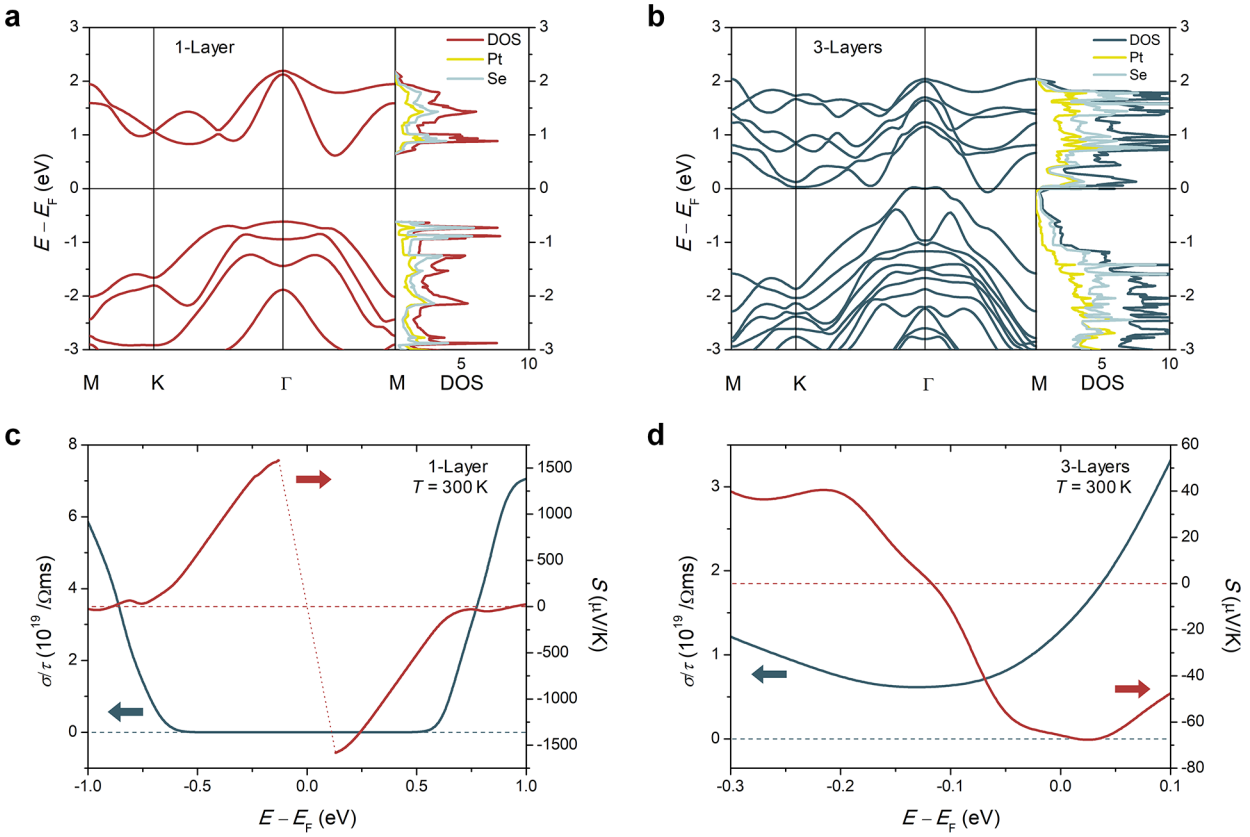

Figure 2. Theoretical calculation of the electronic properties of the $PtSe_2$ nanosheets. (a, b) Electronic band structures and DOS of monolayer (a) and trilayer (b) $PtSe_2$ nanosheets. (c, d) Electrical conductivity (σ) with respect to scattering time (τ) (dark blue) and thermopower (S) (red) of the monolayer (c) and trilayer (d) nanosheets as a function of the energy at room temperature. The horizontal dashed lines indicate zero-electrical conductivity (dark blue) and zero-thermoelectric power (red). The red dotted line indicates the range where no thermopower could be obtained.

investigate the crystal structure of our samples, we performed high-resolution scanning transmission electron microscopy (HR-STEM). The top and side view HR-STEM images and corresponding Fourier transformation images indicate the single-crystalline nature of the mechanically exfoliated nanosheets (Figure 1c,d and top insets). High-magnification HR-STEM images clearly show bright Pt atoms each surrounded by six dark Se atoms (Figure 1c, bottom inset) and the layered structure of $PtSe_2$ (Figure 1d, bottom inset) indicating the 1T phase of the TMDCs.[30] The lattice constants were found to be a = 0.373 nm and c = 0.508 nm from the observed (100) and (001) plane spacings, which is in good agreement with a previous study.[31]

Semimetal to Semiconductor Transition in PtSe2 Nanosheets. In order to calculate the thickness-modulated band structures and the critical thickness of the semimetal to semiconductor transition in $PtSe_2$ nanosheets, we performed first-principle calculations using density functional theory (DFT). We found that the band structure and density of states (DOS) of a monolayer $PtSe_2$ nanosheet represent those of an indirect semiconductor with a bandgap (E_g = 1.23 eV, Figure 2a), which is in good agreement with previous theoretical studies of the same system.[27,30] In a bilayer nanosheet, the bandgap was reduced to 0.23 eV (Figure S1). In the trilayer nanosheet, conduction and valence bands started to overlap (E_0 = 0.09 eV, Figure 2b), thus exhibiting a semimetallic band structure. This is due to the new energy states originating from an extremely strong interlayer p_z orbital hybridization of the Se atom, in which the antibonding p_z states are higher than the valence band maximum of a monolayer.[30] The band structure changed continuously with an increasing number of layers due to an increase of the antibonding p_z states. Bulk $PtSe_2$ exhibited a semimetallic band structure with an indirect band overlap of 0.87 eV (Figure S1).

To calculate the transport properties of monolayer and trilayer nanosheets, we solved the Boltzmann transport equation based on the DFT calculations (Figure 2c,d). In the monolayer nanosheet with a bandgap, the estimated electrical conductivity clearly showed semiconducting characteristics (Figure 2c). We predicted an enhancement of the thermopower above 1 mV/K near the conduction and valence band edges. The trilayer nanosheets with a semimetallic band structure, wherein electrons and holes coexist, exhibited ambipolar transport characteristics (Figure 2d). Near the overlapping bands, the electrical conductivity showed a minimum value without off (high resistance) state, and the thermopower changed signs by passing through zero thermopower. This is because the thermopower of electrons (S < 0) and holes (S > 0) offset each other.[32] For this reason, in semimetals, a significant enhancement of thermopower is hardly observed. This limitation caused by the ambipolar transport effect can be dealt with by introducing an SMSC transition, which leads to the formation of a bandgap. Consequently, we found significant changes in transport characteristics when varying the thickness from bulk to

DOI: 10.1021/acsnano.9b06523
ACS Nano 2019, 13, 13317−13324

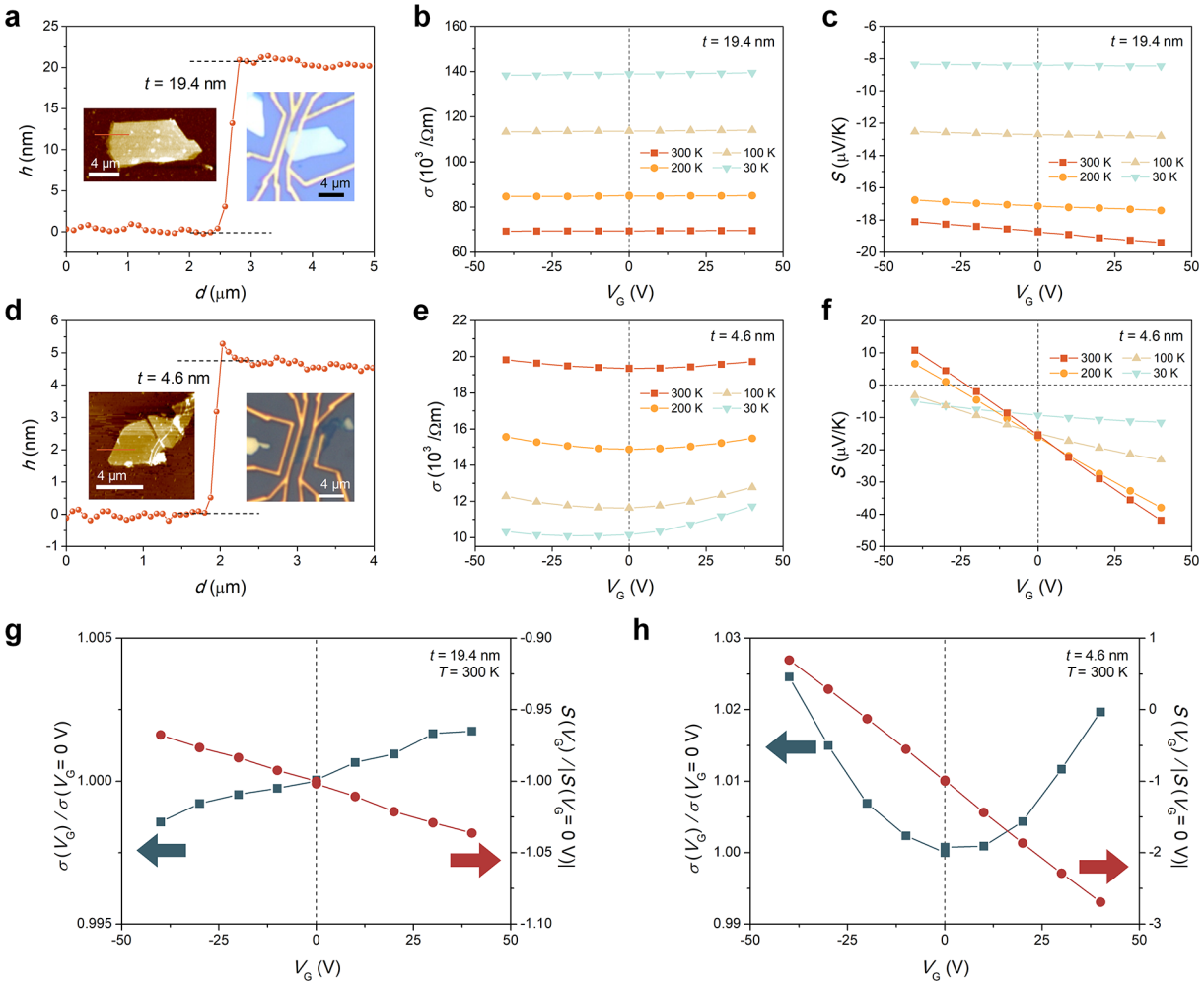

Figure 3. Transport characterization of 19.4 nm-thick and 4.6 nm-thin $PtSe_2$ nanosheets. (a, d) AFM height profiles of the thick (a) and thin (d) $PtSe_2$ nanosheets. The left and right insets show the nanosheets before (as a topographic AFM image) and after device fabrication (as an optical image), respectively. (b, e) Gated electrical conductivity of the thick (b) and thin (e) nanosheets at 300 K (red squares), 200 K (orange circles), and 100 K (khaki triangles) and 30 K (light blue downward facing triangles). (c, f) Gated thermopower of the thick (c) and thin (f) nanosheets at the same temperatures. The error bars are smaller than the symbol size. (g, h) Normalized electrical conductivity (dark blue squares) and thermopower (red circles) with respect to the gate voltage of the thick (g) and thin (h) nanosheets at room temperature.

monolayer, resulting in a dramatic thermopower enhancement (Figure S2).

Semimetallic PtSe2 Nanosheets. To test our theoretical simulations of semimetallic TMDCs and to examine the efficiency of the band engineering approach for transport modulation, we investigated the transport properties of semimetallic $PtSe_2$ nanosheets with more than three layers. In the following, we refer to $PtSe_2$ nanosheets with a thickness of 19.4 nm to "thick nanosheets" and to those with a thickness of 4.6 nm to "thin nanosheets". According to the layer spacing, the layer numbers of the thick and thin nanosheets were estimated to be 38 and 9, respectively. The devices for electrical conductivity and thermopower measurements were fabricated with exfoliated $PtSe_2$ nanosheets by lithography and metallization after determining the thickness using atomic force microscopy (AFM, Figure 3a,d). The measurement errors were negligible compared to the variation of transport properties according to the temperature and gate voltage (Figures S4–S6). We also found that the transport properties of the $PtSe_2$ nanosheets were stable and reproducible (Figures S7 and S8).

The electrical conductivity of the thick nanosheets increased with decreasing temperature, and we hardly observed gate-modulated variation (Figure 3b). The sample, thus, exhibited metal-like transport characteristics. These findings indicate that a highly degenerate band structure with sufficient charge density was present and that they are consistent with a previous study on a $PtSe_2$ nanosheet thicker than 10 nm obtained from the same $PtSe_2$ crystals.[28] Moreover, the carrier-surface scattering in the thick nanosheets was not large enough to suppress the temperature dependence of the carrier mobility, which is the reason why the temperature-dependent electrical conductivity exhibited the metallic behavior.[17,30] The thermopower of the thick nanosheets showed negative values with very weak gate dependence at the voltage range of −40 to 40 V (Figure 3c), which means that electrons are the major charge carriers. Normalizing the electrical conductivity and thermopower demonstrated a weak gate-modulated character of the thick nanosheets (Figure 3g). The gate-modulated electrical conductivity had a positive slope, which indicates electron-dominant transport; the absolute value of the thermopower increased with increasing electron density. This

DOI: 10.1021/acsnano.9b06523
ACS Nano 2019, 13, 13317−13324

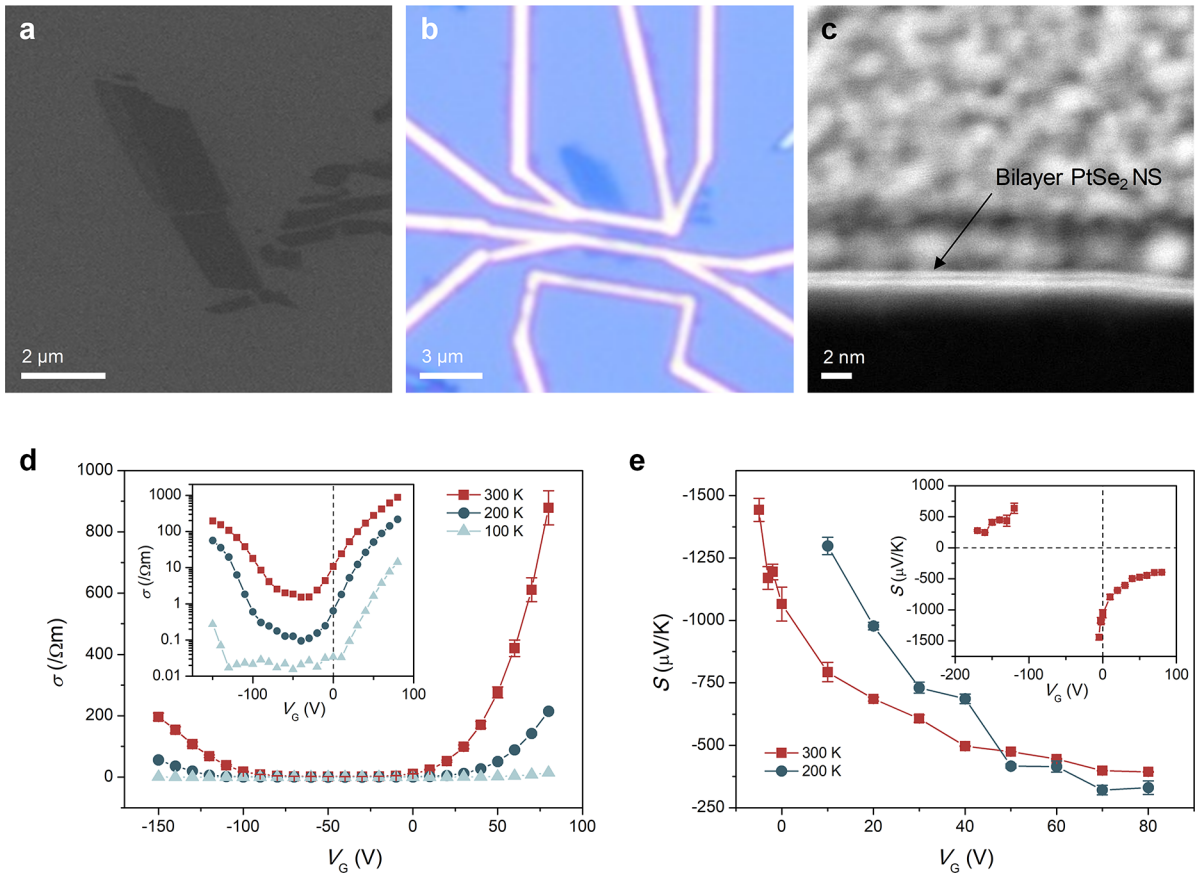

Figure 4. Transport characterization of an ultrathin bilayer $PtSe_2$ nanosheet. (a) Scanning electron microscopy (SEM) image before device fabrication. (b) Optical image after device fabrication. (c) Cross-sectional STEM image of a vertically sliced specimen of the device after the transport measurements. (d) Gated electrical conductivity at 300 K (red squares), 200 K (dark blue circles), and 100 K (light blue triangles). The inset shows the same graph in log scale. (e) Gated thermopower in a gate voltage range of −5 to 80 V. The inset shows the gated thermopower in the whole tested gate voltage range of −170 to 80 V reflecting the semiconducting band structure.

metal-like behavior was consistently observed in nanosheets thicker than 40 nm (Figure S9) and is in good agreement with the theoretical calculation of the carrier density-dependent transport properties in bulk $PtSe_2$ (Figure S3).

The gate-modulated electrical conductivity and thermopower of the thin $PtSe_2$ nanosheets showed ambipolar transport characteristics, as predicted from the semimetallic band structures (Figure 3e, f). The normalized data showed that the electrical conductivity of the thin nanosheet exhibited a u-shape nonmonotonic variation with respect to the gate voltage (Figure 3h). This is a strong evidence for ambipolar transport that is due to an indirect band overlap of semimetals as shown in the theoretical calculation (Figure 2d) and is in good agreement with a previous study using the polymer electrolyte gate effect on 4 and 5 nm nanosheets obtained from the same $PtSe_2$ crystals.[28] The positive and negative slopes of the gate-modulated electrical conductivity indicate electron- and hole-dominant transport, respectively. The thermopower also changed continuously from positive to negative as the gate voltage increased, and the major carriers vary from holes to electrons, as shown in the calculation (Figure 2d). This ambipolar transport behavior can be understood with a two band model in semimetals (Figure S10).[5,17]

It should be noted that the thick nanosheet with bulk characteristics does not show clear ambipolar transport characteristics even in the semimetallic band structure. This can be attributed to the difference of band overlap energy in the nanosheets with different thicknesses. As shown in the theoretical predictions, bulk $PtSe_2$ is also a semimetal (Figure S1) and exhibits ambipolar transport within the energy of the band overlap (Figure S2). However, in terms of a variation in the carrier density, the change in transport properties of bulk $PtSe_2$ is significantly weaker than that of the trilayer nanosheet (Figure S3). This is because the band overlap energy of bulk $PtSe_2$ (0.87 eV) is larger than that of the trilayer nanosheets (0.09 eV). The widening band overlap leads to an increase of carrier density.[33] Thus, despite the same variation in carrier density as in the case of the trilayer, only electron dominant transport is observed in the bulk. In the thin nanosheets, a temperature dependence of the electrical conductivity due to thermally excited charge carriers can be observed because the reduced band overlap decreases the carrier density (Figure 3e). The gate-modulated variations of electrical conductivity and thermopower in the thin nanosheet were 10 and 40 times larger than those of the thick nanosheet, respectively (Figure 3g,h). This suggests that the thickness-modulated band engineering based on semimetallic $PtSe_2$ is sufficient to effectively tune the transport properties in nanosheets.

Semiconducting PtSe2 Nanosheets. In order to determine the largest thermopower enhancement in $PtSe_2$ nanosheets and to evaluate potential thermoelectric applications of the thickness-modulated band-engineered semimetallic TMDCs, we investigated the thinnest $PtSe_2$ nanosheets we were able to produce, a bilayer nanosheet. We first fabricated

DOI: 10.1021/acsnano.9b06523
ACS Nano 2019, 13, 13317−13324

the microdevice for transport measurements using this ultrathin nanosheet (Figure 4a,b). The number of layers was determined by cross-sectional STEM of a specimen sliced vertically after the transport measurements because absorbents on the surfaces of substrate and nanosheet can cause an overestimation of the AFM height profile in atomically thin nanosheets (Figure 4c).[34,35] The gate-modulated electrical conductivity of the ultrathin nanosheet showed clear semiconducting characteristics with on/off states indicating the formation of a bandgap (Figure 4d).[30] We successfully conducted a sufficient gate voltage sweep of −150 to 80 V, and we were able to observe the electron and hole dominant transport on both sides of the bandgap in the temperature range of 100 to 300 K (inset of Figure 4d). This is consistent with the previously observed polymer electrolyte gate effect on a 2.5 nm nanosheet obtained from the same $PtSe_2$ crystals.[28]

To confirm the predicted thermopower enhancement, we examined the variation of thermopower with the gate voltage sweep of −5 to 80 V (Figure 4e). As approaching the off state, the absolute value of the thermopower sharply increased to 1.5 mV/K in the measurable range, which is more than 50 times larger than that of the metal-like thick nanosheet. We note that in the off state, the reduced electrical conductivity decreased the signal-to-noise ratio of the thermopower voltage, increasing measurement errors (Figures S4−S6). Furthermore, in the full range gate voltage sweep (−170 to 80 V), we clearly observed the theoretically predicted changes in positive and negative thermopower on both sides of the off state (inset of Figure 4e), which originate from hole and electron bands, respectively (Figure 2c).

Tunable Thermoelectric Performance. Finally, to evaluate the enhancement of thermoelectric performance in thickness-modulated band-engineered $PtSe_2$ nanosheets, we obtained the power factor from the measured electrical conductivity and thermopower. We fabricated and measured three additional devices with four-probe measurements to eliminate any deviation due to contact resistance and to determine the variation of the power factor originating from the band engineering (Figure S11). Prior to the SMSC transition, the power factor gradually decreased with decreasing nanosheet thickness due to carrier-surface scattering and ambipolar transport, except for the 19.4 nm nanosheet where the electrical conductivity was underestimated owing to contact resistance (Figure 5). However, the variation of the power factor according to the gate voltage increased rapidly with decreasing band overlap energy (inset of Figure 5), and in the bilayer nanosheet, the value sharply increased with increasing gate voltage. Moreover, the rate of change in gated electrical conductivity and thermopower indicated that the power factor of the semiconducting nanosheet can be increased further in a higher gate voltage range (Figure 4d,e). Consequently, we demonstrated the enhancement of the power factor and its tunability using an SMSC transition in semimetallic $PtSe_2$.

CONCLUSION

Our study demonstrates a dramatic enhancement of thermopower based on thickness-modulated electronic band engineering using two-dimensional nanosheets exfoliated from semimetallic $PtSe_2$ crystals. The synthetic semiconducting nanosheets obtained by an SMSC transition from semimetallic TMDCs have several advantages for thermoelectric applications such as (1) a large variation of transport properties, (2) a decrease of the ambipolar transport effect, and (3) a high carrier density dependence of the transport properties. While thick $PtSe_2$ nanosheets (19.4 nm) showed metal-like characteristics similar to bulk crystals, a semimetallic ambipolar behavior was observed in thin nanosheets (4.6 nm). With an ultrathin nanosheet (bilayer), we were able to observe apparent semiconducting gating characteristics and, as a result, could obtain thermopower values higher than 1 mV/K and an enhanced and tunable power factor. Our observations suggest the development of thermoelectric applications based on thickness-modulated band engineering of other semimetallic TMDCs. We anticipate that even metallic bulk crystals with poor thermoelectric performances are worth studying to develop promising two-dimensional nanostructured thermoelectric materials.

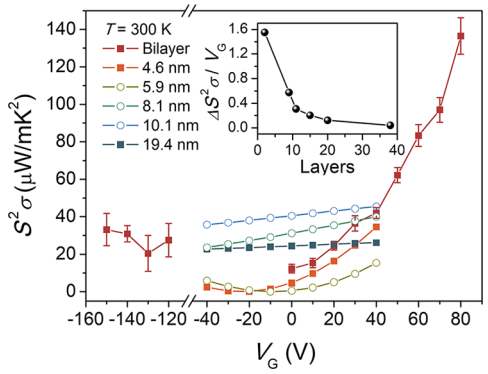

Figure 5. Thermoelectric performance characterization of $PtSe_2$ nanosheets of different thicknesses. Power factors ($S^2\sigma$) of the bilayer (red squares), 4.6 (orange squares), 5.9 (yellow circles), 8.1 (green circles), 10.1 (light blue circles), and 19.4 nm nanosheets (dark blue squares) as a function of the gate voltages at room temperature. Solid and open symbols refer to the use of two- and four-probe measurements to obtain the electrical conductivity, respectively. The error bars were smaller than the symbol size except for the bilayer nanosheet. The inset shows the gate dependence of the power factors as a function of the layer numbers. The unit of $\Delta S^2\sigma/V_G$ is μW/mK^{2}V. The numbers of nanosheet layers were estimated based on their thickness according to the lattice constant of *c*.

EXPERIMENTAL SECTION

Device Fabrication. $PtSe_2$ nanosheets were mechanically exfoliated onto a highly doped Si substrate with 300 nm-thick thermally grown SiO_2 using bulk $PtSe_2$ crystals (HQ Graphene). The layered crystal structure of the exfoliated $PtSe_2$ nanosheets was characterized using STEM (JEM-ARM 200F, Jeol), dual beam FIB (crossbeam 540, ZEISS), and Raman spectroscopy (LabRam ARAMIS, Horiba Scientific). Thickness measurements using AFM (XE-150, Park Systems) were performed before device fabrication to select nanosheets of the desired thicknesses. Microdevices for transport measurements were fabricated using electron-beam lithography (VEGA3, Tescan and NPGS, JC Nabity Lithography Systems) and a lift-off process. To optimize electrical contact between the $PtSe_2$ and the electrodes, the patterned nanosheet was exposed for 20 s to Ar plasma, followed by a Cr (5 nm)/Au (100 nm) metallization using a custom-made plasma etching and sputtering system. Details of the device fabrication are described in previous reports.[17,36]

Band Structure and Transport Property Calculations. First-principle DFT calculations were performed using the projector augmented plane-wave method implemented in the Vienna *ab Initio* simulation program code.[37] The general gradient approximation with the Perdew−Burke−Ernzerhof functional was used with spin−orbit

DOI: 10.1021/acsnano.9b06523
ACS Nano 2019, 13, 13317−13324

coupling.[38,39] Slab supercells of monolayer, bilayer, and trilayer with a vacuum layer of 15 Å along the *c*-axis were used. van der Waals correction was included using the DFT-D3 method with Becke–Johnson rational damping.[40,41] A *k*-point mesh of 56 × 56 × 1 was used for the monolayer, bilayer, and trilayer models, and a 28 × 28 × 28 *k*-point mesh was used for the bulk model. The plane-wave basis cutoff energy was set to 700 eV. The structural relaxations were performed until the Hellmann–Feynman forces were $<10^{-5}$ eVÅ^{-1}. The electrical conductivity and the thermoelectric power were estimated using the Shankland–Koelling–Wood interpolation as implemented in the BoltzTraP2 code.[42,43]

Transport Property Measurements. The microdevice for transport property measurements consisted of a microheater and two thermometers. The electrical conductivity was obtained by *I*–*V* and *V*–*I* measurement systems (236 and 2182, Keithley) for low-resistance metal-like and semimetallic nanosheets and for high-resistance semiconducting nanosheets, respectively. For the thermopower measurement, the voltage difference between two thermometers was measured by a nanovoltmeter (2182, Keithley). The temperature difference was calibrated using the temperature coefficient of the resistance of each thermometer, which was measured by a lock-in amplifier (SR850, Stanford Research Systems) during Joule heating of the microheater. All measurements including the temperature-dependent properties were conducted using a closed cycle cryostat (X-1AL, Advanced Research Systems) in a high vacuum of $<5 \times 10^{-6}$ Torr without convectional thermal fluctuation. A detailed description of the transport measurements based on single nanosheets is available in the Supporting Information (Figures S4–S6) and previous studies.[17,32]

ASSOCIATED CONTENT

Supporting Information

The Supporting Information is available free of charge on the ACS Publications website at DOI: 10.1021/acsnano.9b06523.

Calculated electronic band structures, DOS, and transport properties for monolayer, bilayer, trilayer nanosheets, and bulk crystal, measurement techniques and errors with representative raw data, four-probe measurements and contact resistance, stability and reproducibility of $PtSe_2$ nanosheets, transport properties of a metal-like 40 nm nanosheet, and simple two band model in transport properties of semimetals (PDF)

AUTHOR INFORMATION

Corresponding Authors

*E-mail: wooyoung@yonsei.ac.kr.
*E-mail: jmkim@yonsei.ac.kr.

ORCID

Wooyoung Lee: 0000-0001-8406-4324

Notes

The authors declare no competing financial interest.

ACKNOWLEDGMENTS

This work was supported by the National Research Foundation of Korea (NRF) grant funded by the Korea government (MSIT, 2017R1A2A1A17069528).

REFERENCES

(1) Venkatasubramanian, R.; Siivola, E.; Colpitts, T.; O'Quinn, B. Thin-Film Thermoelectric Devices with High Room-Temperature Figures of Merit. *Nature* **2001**, *413*, 597–602.

(2) Hochbaum, A. I.; Chen, R.; Delgado, R. D.; Liang, W.; Garnett, E. C.; Najarian, M.; Majumdar, A.; Yang, P. Enhanced Thermoelectric Performance of Rough Silicon Nanowires. *Nature* **2008**, *451*, 163–167.

(3) Heremans, J. P.; Dresselhaus, M. S.; Bell, L. E.; Morelli, D. T. When Thermoelectrics Reached the Nanoscale. *Nat. Nanotechnol.* **2013**, *8*, 471.

(4) Goldsmid, H. J. *Thermoelectric Refrigeration*; Plenum Press: New York, 1964.

(5) Hicks, L. D.; Dresselhaus, M. S. Effect of Quantum-Well Structures on the Thermoelectric Figure of Merit. *Phys. Rev. B: Condens. Matter Mater. Phys.* **1993**, *47*, 12727–12731.

(6) Dresselhaus, M. S.; Dresselhaus, G.; Sun, X.; Zhang, Z.; Cronin, S. B.; Koga, T. Low-Dimensional Thermoelectric Materials. *Phys. Solid State* **1999**, *41*, 679–682.

(7) Touzelbaev, M. N.; Zhou, P.; Venkatasubramanian, R.; Goodson, K. E. Thermal Characterization of Bi_2Te_3/Sb_2Te_3 Superlattices. *J. Appl. Phys.* **2001**, *90*, 763–767.

(8) Lim, J.; Hippalgaonkar, K.; Andrews, S. C.; Majumdar, A.; Yang, P. Quantifying Surface Roughness Effects on Phonon Transport in Silicon Nanowires. *Nano Lett.* **2012**, *12*, 2475–2482.

(9) Kang, J.; Roh, J. W.; Shim, W.; Ham, J.; Noh, J.-S.; Lee, W. Reduction of Lattice Thermal Conductivity in Single Bi-Te Core/Shell Nanowires with Rough Interface. *Adv. Mater.* **2011**, *23*, 3414–3419.

(10) Yu, J.-K.; Mitrovic, S.; Tham, D.; Varghese, J.; Heath, J. R. Reduction of Thermal Conductivity in Phononic Nanomesh Structures. *Nat. Nanotechnol.* **2010**, *5*, 718.

(11) Mao, J.; Liu, Z.; Ren, Z. Size Effect in Thermoelectric Materials. *npj Quantum Mater.* **2016**, *1*, 16028.

(12) Chen, R.; Lee, J.; Lee, W.; Li, D. Thermoelectrics of Nanowires. *Chem. Rev.* **2019**, *119*, 9260.

(13) Kim, J.; Shim, W.; Lee, W. Bismuth Nanowire Thermoelectrics. *J. Mater. Chem. C* **2015**, *3*, 11999–12013.

(14) Heremans, J.; Thrush, C. M. Thermoelectric Power of Bismuth Nanowires. *Phys. Rev. B: Condens. Matter Mater. Phys.* **1999**, *59*, 12579–12583.

(15) Boukai, A. I.; Bunimovich, Y.; Tahir-Kheli, J.; Yu, J.-K.; Goddard, W. A., Iii; Heath, J. R. Silicon Nanowires as Efficient Thermoelectric Materials. *Nature* **2008**, *451*, 168.

(16) Shapira, E.; Holtzman, A.; Marchak, D.; Selzer, Y. Very High Thermopower of Bi Nanowires with Embedded Quantum Point Contacts. *Nano Lett.* **2012**, *12*, 808–812.

(17) Kim, J.; Lee, S.; Brovman, Y. M.; Kim, P.; Lee, W. Diameter-Dependent Thermoelectric Figure of Merit in Single-Crystalline Bi Nanowires. *Nanoscale* **2015**, *7*, 5053–5059.

(18) Yoshida, M.; Iizuka, T.; Saito, Y.; Onga, M.; Suzuki, R.; Zhang, Y.; Iwasa, Y.; Shimizu, S. Gate-Optimized Thermoelectric Power Factor in Ultrathin WSe_2 Single Crystals. *Nano Lett.* **2016**, *16*, 2061–2065.

(19) Hippalgaonkar, K.; Wang, Y.; Ye, Y.; Qiu, D. Y.; Zhu, H.; Wang, Y.; Moore, J.; Louie, S. G.; Zhang, X. High Thermoelectric Power Factor in Two-Dimensional Crystals of MoS_2. *Phys. Rev. B: Condens. Matter Mater. Phys.* **2017**, *95*, 115407.

(20) Park, M.; Hong, S. J.; Kim, K. H.; Kang, H.; Lee, M.; Jeong, D. H.; Park, Y. W.; Kim, B. H. Electrical and Thermoelectric Transport by Variable Range Hopping in Reduced Graphene Oxide. *Appl. Phys. Lett.* **2017**, *111*, 173103.

(21) Wickramaratne, D.; Zahid, F.; Lake, R. K. Electronic and Thermoelectric Properties of Few-Layer Transition Metal Dichalcogenides. *J. Chem. Phys.* **2014**, *140*, 124710.

(22) Huang, W.; Luo, X.; Gan, C. K.; Quek, S. Y.; Liang, G. Theoretical Study of Thermoelectric Properties of Few-Layer MoS_2 and WSe_2. *Phys. Chem. Chem. Phys.* **2014**, *16*, 10866–10874.

(23) Li, J.; Shen, J.; Ma, Z.; Wu, K. Thickness-Controlled Electronic Structure and Thermoelectric Performance of Ultrathin SnS_2 Nanosheets. *Sci. Rep.* **2017**, *7*, 8914.

(24) Zhang, R.-z.; Wan, C.-l.; Wang, Y.-f.; Koumoto, K. Titanium Sulphene: Two-Dimensional Confinement of Electrons and Phonons Giving Rise to Improved Thermoelectric Performance. *Phys. Chem. Chem. Phys.* **2012**, *14*, 15641–15644.

DOI: 10.1021/acsnano.9b06523
ACS Nano 2019, 13, 13317–13324

(25) Kumar, S.; Schwingenschlögl, U. Thermoelectric Response of Bulk and Monolayer $MoSe_2$ and WSe_2. *Chem. Mater.* **2015**, *27*, 1278−1284.
(26) Buscema, M.; Barkelid, M.; Zwiller, V.; van der Zant, H. S. J.; Steele, G. A.; Castellanos-Gomez, A. Large and Tunable Photothermoelectric Effect in Single-Layer MoS_2. *Nano Lett.* **2013**, *13*, 358−363.
(27) Guo, S.-D. Biaxial Strain Tuned Thermoelectric Properties in Monolayer $PtSe_2$. *J. Mater. Chem. C* **2016**, *4*, 9366−9374.
(28) Ciarrocchi, A.; Avsar, A.; Ovchinnikov, D.; Kis, A. Thickness-Modulated Metal-to-Semiconductor Transformation in a Transition Metal Dichalcogenide. *Nat. Commun.* **2018**, *9*, 919.
(29) O'Brien, M.; McEvoy, N.; Motta, C.; Zheng, J.-Y.; Berner, N. C.; Kotakoski, J.; Elibol, K.; Pennycook, T. J.; Meyer, J. C.; Yim, C.; Abid, M.; Hallam, T.; Donegan, J. F.; Sanvito, S.; Duesberg, G. S. Raman Characterization of Platinum Diselenide Thin Films. *2D Mater.* **2016**, *3*, 021004.
(30) Zhao, Y.; Qiao, J.; Yu, Z.; Yu, P.; Xu, K.; Lau, S. P.; Zhou, W.; Liu, Z.; Wang, X.; Ji, W.; Chai, Y. High-Electron-Mobility and Air-Stable 2d Layered $PtSe_2$ FETs. *Adv. Mater.* **2017**, *29*, 1604230.
(31) Zhang, K.; Yan, M.; Zhang, H.; Huang, H.; Arita, M.; Sun, Z.; Duan, W.; Wu, Y.; Zhou, S. Experimental Evidence for Type-Ii Dirac Semimetal in $PtSe_2$. *Phys. Rev. B: Condens. Matter Mater. Phys.* **2017**, *96*, 125102.
(32) Kim, J.; Yoo, S.; Moon, H.; Kim, S. Y.; Ko, D.-S.; Roh, J. W.; Lee, W. Ambipolar Thermoelectric Power of Chemically-Exfoliated RuO_2 Nanosheets. *Nanotechnology* **2018**, *29*, 015404.
(33) Kim, J.; Kim, D.; Chang, T.; Lee, W. Quantum Size Effect on Shubnikov-De Haas Oscillations in 100 nm Diameter Single-Crystalline Bismuth Nanowire. *Appl. Phys. Lett.* **2014**, *105*, 123107.
(34) Li, H.; Zhang, Q.; Yap, C. C. R.; Tay, B. K.; Edwin, T. H. T.; Olivier, A.; Baillargeat, D. From Bulk to Monolayer MoS_2: Evolution of Raman Scattering. *Adv. Funct. Mater.* **2012**, *22*, 1385−1390.
(35) Shearer, C. J.; Slattery, A. D.; Stapleton, A. J.; Shapter, J. G.; Gibson, C. T. Accurate Thickness Measurement of Graphene. *Nanotechnology* **2016**, *27*, 125704.
(36) Yoo, S.; Kim, J.; Moon, H.; Kim, S. Y.; Ko, D.-s.; Shin, W. H.; Hwang, S.; Jung, D. W.; Sul, S.; Kwak, C.; Roh, J. W.; Lee, W. Strong Enhancement of Electrical Conductivity in Two-Dimensional Micrometer-Sized RuO_2 Nanosheets for Flexible Transparent Electrodes. *Nanoscale* **2017**, *9*, 7104−7113.
(37) Kresse, G.; Furthmüller, J. Efficient Iterative Schemes for *Ab Initio* Total-Energy Calculations Using a Plane-Wave Basis Set. *Phys. Rev. B: Condens. Matter Mater. Phys.* **1996**, *54*, 11169−11186.
(38) Perdew, J. P.; Burke, K.; Ernzerhof, M. Generalized Gradient Approximation Made Simple. *Phys. Rev. Lett.* **1996**, *77*, 3865−3868.
(39) Steiner, S.; Khmelevskyi, S.; Marsmann, M.; Kresse, G. Calculation of the Magnetic Anisotropy with Projected-Augmented-Wave Methodology and the Case Study of Disordered $Fe_{1-X}Co_x$ Alloys. *Phys. Rev. B: Condens. Matter Mater. Phys.* **2016**, *93*, 224425.
(40) Grimme, S.; Antony, J.; Ehrlich, S.; Krieg, H. A Consistent and Accurate *Ab Initio* Parametrization of Density Functional Dispersion Correction (Dft-D) for the 94 Elements H-Pu. *J. Chem. Phys.* **2010**, *132*, 154104.
(41) Grimme, S.; Ehrlich, S.; Goerigk, L. Effect of the Damping Function in Dispersion Corrected Density Functional Theory. *J. Comput. Chem.* **2011**, *32*, 1456−1465.
(42) Pickett, W. E.; Krakauer, H.; Allen, P. B. Smooth Fourier Interpolation of Periodic Functions. *Phys. Rev. B: Condens. Matter Mater. Phys.* **1988**, *38*, 2721−2726.
(43) Madsen, G. K. H.; Carrete, J.; Verstraete, M. J. Boltztrap2, a Program for Interpolating Band Structures and Calculating Semi-Classical Transport Coefficients. *Comput. Phys. Commun.* **2018**, *231*, 140−145.

DOI: 10.1021/acsnano.9b06523
ACS Nano 2019, 13, 13317−13324